National Physical Laboratory

NPL REPORT MAT 83

CHARACTERISATION OF INITIATION SITES FOR CRACKS DEVELOPED FROM PITS IN A SHOT-PEENED 12Cr BLADE STEEL

L. GUO, S. ZHOU, L. CROCKER AND A. TURNBULL

NOVEMBER 2016

Department for Business, Energy & Industrial Strategy

FUNDED BY BEIS

Characterisation of initiation sites for cracks developed from pits in a shot-peened 12Cr blade steel

Liya Guo, Shengqi Zhou, Louise Crocker and Alan Turnbull
Materials Division

ABSTRACT

A serial sectioning procedure was carried out on a shot-peened 12Cr martensitic stainless steel to determine the location of fatigue crack initiation sites from pits of varying depth. Multiple cracks, including fully-developed cracks (surface-breaking cracks extending beyond the pit base) and non-fully-developed cracks, were observed for pits of depth greater than 70 μm. If the longest crack at each side of the pit was assumed to be the “dominant” crack, most “dominant” cracks did not initiate near the pit base despite a propensity for macro-stress and strain localisation to the pit base.

ISSN 1754-2979

National Physical Laboratory
Hampton Road, Teddington, Middlesex, TW11 0LW

Approved on behalf of NPLML by Prof. Mark Gee,
Knowledge Leader, Materials Division

CONTENTS

1 INTRODUCTION

In the steam turbine industry, shot peening is commonly applied to engineering components to induce a residual compressive stress field into the surface of the metal and thereby increase the fatigue life. Most research has focused on the beneficial effect of the shot-peened surface [1-3]. However, where cracks develop from corrosion pits there is significant uncertainty as to the residual benefit of shot peening, especially when the pit depth approaches that of the compressive stress layer. While there is awareness of this possibility there has been surprisingly little research to investigate the effect of pitting corrosion on the fatigue life of shot-peened components. Characterisation of crack evolution from pits on shot-peened specimens in the early stages is required to provide understanding of the damage development process. In previous research on crack initiation sites on shot-peened specimens with pits, notches/artificial pits were introduced by electrical discharge machining [4, 5], or by drilling to a certain size followed by metal dissolution with nitric acid [6]. Artificial pits generated by these methods may not be representative of the macro-geometry of real pits. Also, a real pit will exhibit microtopographical features that would be expected to affect the stress/strain distribution at a local level [7] and consequently the crack initiation site.

In this report, an effort has been made to determine the site/s of fatigue crack initiation from "real" pits in shot-peened 12Cr martensitic stainless steel. Pits with a range of depths on the same specimen were generated electrochemically to explore the possible effect of pit size on the fatigue crack initiation site, the idea being to capture the early stages of crack development before the cracks were fully developed and information about the initiation location lost. Consequently, the approach was to undertake interrupted fatigue tests with the intent of capturing the onset of a crack before it had grown to a size similar to that of the pit.

2 EXPERIMENTAL PROCEDURE

Eight pits (positioned in a line, parallel to the stress axis and about 1-2 mm apart)) with different depth ranging from 30 μm to 240 μm were produced on a shot-peened (according to the procedure S170 8-12A) flat dog-bone tensile specimen (FV566) using a galvanostatic droplet technique [8], which had been shown to replicate well the geometrical features of pits in service. The composition of FV566 is shown in Table 1.

Table 1: Composition of FV566 steel (in mass %).

Steel	**C**	**Si**	**Mn**	**P**	**S**	**Cr**	**Mo**	**Ni**	**V**	**N_b**	**Fe**
Composition	0.12	0.30	0.86	0.013	0.002	11.73	1.64	2.59	0.28	0.13	Bal

Fatigue tests, with a sinusoidal wave form, a frequency of 1 Hz and a stress ratio of 0.1 were carried out in air using an Instron 8801 Fatigue Testing Machine. The initial maximum stress (σ_{max}) was 622 MPa (76% $\sigma_{0.2}$); no cracks were observed after 112000 cycles. The maximum stress was subsequently increased to 663 MPa (81% $\sigma_{0.2}$). Fatigue testing was undertaken until a surface crack of ~2.5 mm in length was detected on the deepest pit, at which point the testing was stopped. A preliminary examination of the specimen for cracks was undertaken in a scanning electron microscope (SEM) and the specimen then ultrasonically-cleaned with Super Clarke's solution (5 g/l of 1,3-di-n-butyl-2-thiourea in 18.9% HCl) for 1 hour, followed by ultrasonic cleaning with a solution of 32 g/l of $KMnO_4$ and 100 g/l of NaOH at 80 °C for 15 minutes. The depth of the pits on the specimen was measured by a Nikon Measuring Microscope (MM-60) before and after chemical cleaning and there was no significant change.

In the absence of high resolution X-ray computed tomography, a serial sectioning technique was used to study the crack initiation sites. The specimen and four metal balls with a diameter of 2500 μm were mounted in bakelite. The specimen was then polished layer by layer and the final surface was polished to a 1 μm diamond suspension at the end of each serial sectioning step. The diameters of the four metal

balls were measured after each serial sectioning step to calculate the depth of material removed from the specimen. An average of the values obtained from the four metal balls was used to determine the removed depth. Since the metal balls were not revealed until the first serial sectioning step, the removed depth of the first step was estimated by the depth difference of one pit before and after the serial sectioning process.

3 RESULTS AND DISCUSSION

3.1 CHARACTERISATION OF PIT DEPTH

Table 2 shows the total removed depth of the shot-peened specimen after each serial sectioning step. The depth of the material removed during each step varied from 7 μm to 41 μm with the mean being 16 μm. The specimen was examined in the SEM after each step. The sequence of polishing and subsequent examination was continued until the pit was not observed.

Table 2: Polishing steps and the corresponding depth of material removed from the shot-peened specimen after each serial sectioning step.

Step	**Total depth removed (μm)**
1	20±1
2	27±3
3	36±2
4	51±1
5	64±2
6	82±3
7	93±4
8	103±3
9	114±3
10	133±6
11	174±8
12	201±3
13	216±4
14	231±2
15	242±5

Table 3 shows a range of pits and the corresponding depth of material removed at which the pits were last observed (the second column in the table) and first absent (the third column) during the serial sectioning process. The fourth column shows the pit depth estimated from the mean of these two values. The fifth column in Table 3 shows the depth of pits measured by optical microscopy (OM). For a few pits there was some discrepancy between the estimates from microscopy and those derived from serial sectioning. For example, Pit 6 was estimated to have a depth of 185 μm according to microscopy measurements. However, the pit was still observed after a depth removal of 201±3 μm. This might be caused by error in pit depth measurement through uneven surface polishing during serial sectioning process or because of local variations in geometry of the base that might not have been picked up readily in microscopic measurement (the uncertainty of OM measurement is ±0.5 μm). In this report, the depth of pits refers to the mean value from sectioning.

Table 3: Depth of pits examined by optical microscopy (OM) before serial sectioning and the corresponding depths estimated by averaging the removed depths where the pit was last observed and first absent.

Pit number	Last presence after depth removal of (µm)	First absence after depth removal of (µm)	Pit depth from sectioning (µm)	Pit depth (OM) (µm)
1	27±3	36±2	31±7	36
2	64±2	82±3	74±12	71
3	82±3	93±4	88±9	83
4	114±3	133±6	125±14	96
5	174±8	201±3	185±19	172
6	201±3	216±4	209±11	185
7	216±4	231±2	224±11	191
8	231±2	242±5	238±9	230

3.2 CHARACTERISATION OF CRACKING FROM PITS

Cracks were observed for pits with pit depths varying from 70 µm to 240 µm but no crack was observed for the pit of 31 µm depth.

Figure 1 shows a pit (with irregular shape and microtopographical features) and the corresponding multiple cracks at the left side of the pit. Crack length refers to the length between the edge of the pit and the crack tip, as shown in Figure 1. In this study, a crack is defined as such only when the crack length is greater than 5 µm.

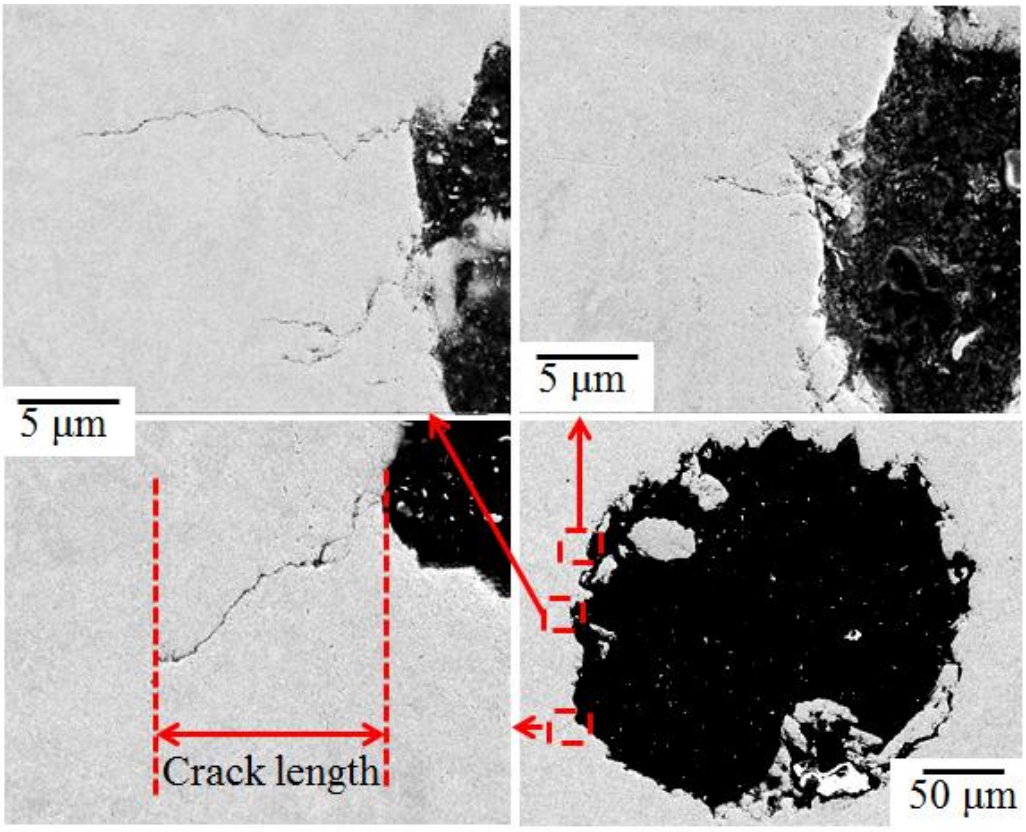

Figure 1: SEM images of a pit of 209 µm depth and the corresponding cracks with a layer removal of 51 µm.

It is apparent in Figure 1 that there are several cracks with a layer removal of 51 μm. Also, new cracks may emerge at greater depths. In longer term testing, one crack tends to dominate. In this interrupted test, it is not possible to identify which crack will become dominant but as a default it is assumed to be the longest crack measured in the direction perpendicular to the stress axis. Figure 2 is a schematic diagram showing a pit (highlighted in grey) and two cracks (highlighted in orange and green) at the left side of the pit. As shown in Figure 2, the maximum length of crack 1 is greater than that of crack 2. Accordingly, this was assumed to be the dominant crack on the left side of the pit.

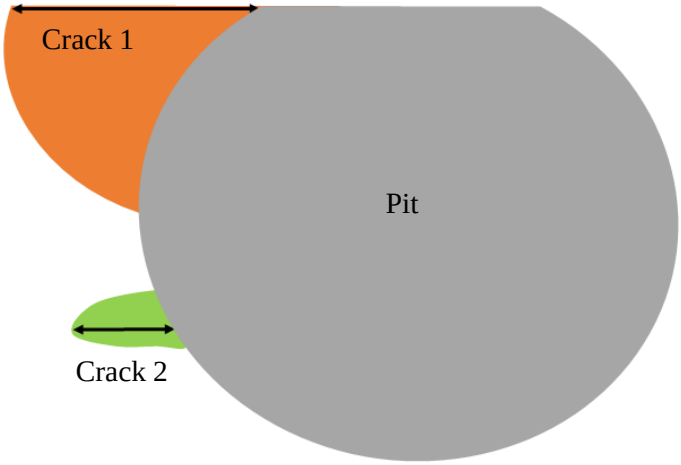

Figure 2: Schematic diagram illustrating the definition of the "dominant" crack with the arrows representing the maximum length of each crack.

It requires much luck in testing to observe the crack just after initiation in order to define the specific location. Nevertheless, since the serial section gives a depth profile we can infer the region round the pit where the crack must have initiated even though the specific location is unknown. On this basis, the ratio of crack depth range to pit depth can be used to reveal the location of a crack relative to the location of the pit from which the crack evolves. Figure 3 shows one pit (the depth of which is 'p') and two cracks at the left side. 'Crack 1' can be observed from the surface until distance 'a' away from the surface. For 'Crack 1', the ratio of crack depth to pit depth ranges from '0' to '$\frac{a}{p}$'. 'Crack 2' can be observed from distance 'b' away from the surface to distance 'c' away from the surface. For 'Crack 2', the ratio of crack depth to pit depth ranges from '$\frac{b}{p}$' to '$\frac{c}{p}$'. By this definition, for a fully-developed crack, the ratio of crack depth to pit depth will range from '0' to '1'. The serial section by its nature has a degree of uncertainty in crack depth, dependent on the depth of material removed. In estimating the crack depth range in this study the mean value of the crack depth was used (Column 4 in Table 3).

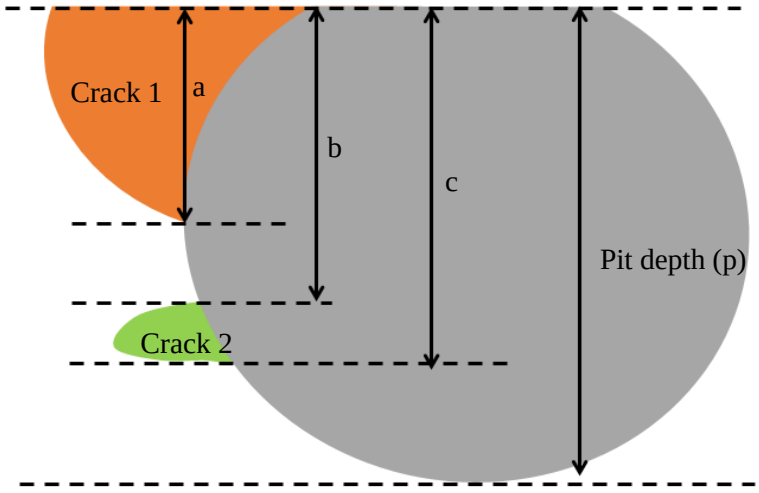

Figure 3: Schematic diagram illustrating the ratio of crack depth range to pit depth.

Figure 4 gives a summary of the ratio of crack depth range to pit depth of the "dominant" cracks associated with the seven pits studied, with pit depths ranging from 70 μm to 240 μm. "Right" crack refers to the "dominant" crack at the right side of the pit and "left" crack refers to the "dominant" crack at the left side of the pit. As shown in Figure 4, fully-developed cracks (the ratio of crack depth range to pit depth being '0' to '1') were only observed for pits with a depth of 209 μm and 238 μm. In addition to fully-developed cracks, non-fully-developed cracks, including surface-breaking cracks (the ratio of crack depth range to pit depth starting from '0' but not ending in '1') were observed. Also, some cracks initiated below the surface but were not surface-breaking (the ratio of crack range to pit depth ending in '1' but not starting from '0').

The crack initiation site cannot be determined for fully-developed cracks. For non-fully-developed cracks, there is uncertainty in determining the exact crack initiation site. For example, the crack initiation site for surface-breaking cracks might not be at the surface since cracks may initiate at the subsurface and then propagate to the surface. It is apparent from Figure 4 that for depths less than about 185 μm none of the cracks observed initiated at the base of the pit, though for the 125 μm pit the initiation site conceivably could have been near the base. At greater pit depths it is more random. Thus, for pits of order of 209 μm there are examples of cracks initiating quite near the surface (0 to 0.4) yet also cracks initiating near to or at the base (about 0.7 to 1). In fact, the latter example is the only one that gives clear evidence of a "dominant" crack initiating near the base. Most of the meaningful observations indicate that cracks do not initiate very close to the base of the pit.

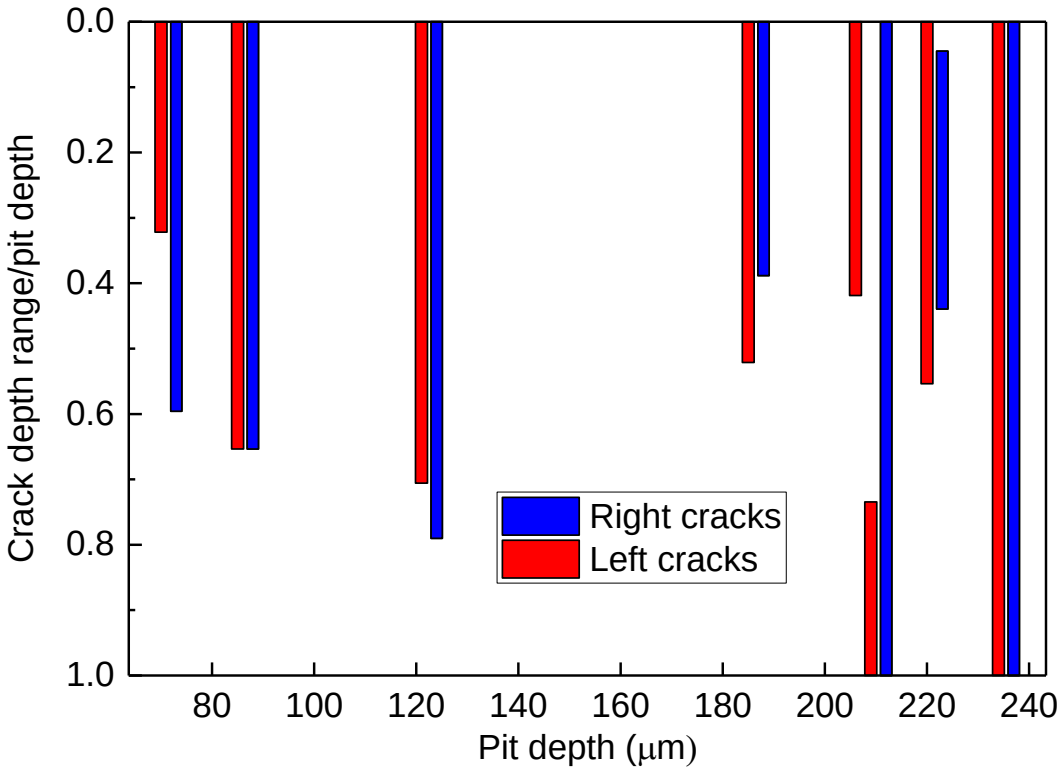

Figure 4: Ratio of crack depth range to pit depth versus pit depth (mean value from sectioning) for "dominant" cracks associated with pits with depths varying from 70 μm to 240 μm.

Figure 5 shows a series of section images for a pit of 74 μm depth and a propagating surface-breaking crack on the right of the pit. This is taken as an example to demonstrate that cracks might initiate near the pit surface and not at the pit base. A surface crack was first observed after fatigue testing, before serial sectioning. The crack can be seen after layer removal steps of 20 μm, 27 μm and 36 μm, while it was absent after a further serial sectioning step.

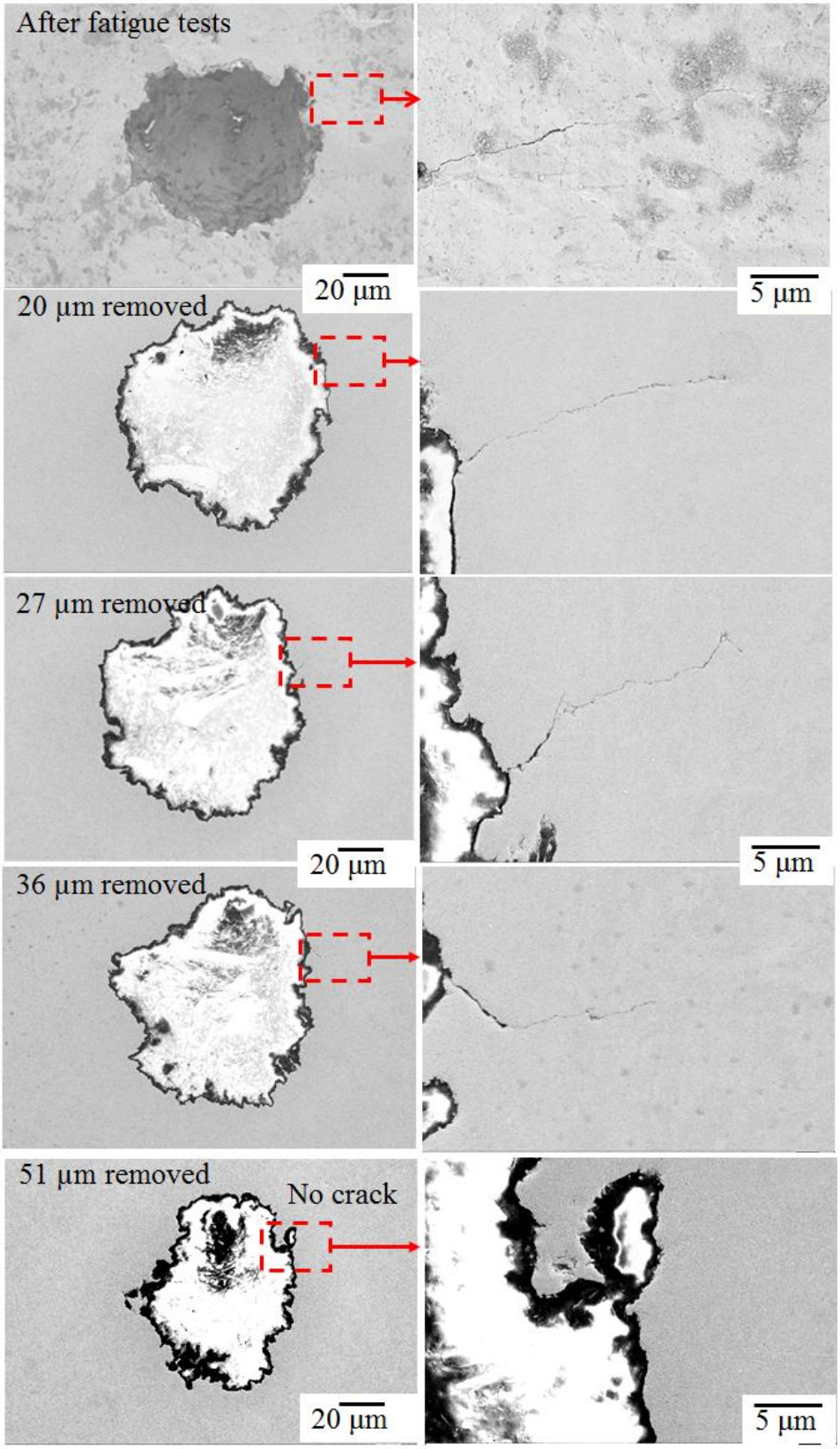

Figure 5: SEM images of a pit of 74 µm depth and a crack observed after fatigue tests and following serial sectioning steps.

In addition to the surface-breaking cracks, Figure 4 shows that a crack might initiate near the pit base. Figure 6 is an example showing crack initiation near the base of a pit of 209 µm depth. After a layer removal of 133 µm and 174 µm, all of the cracks at the left side of the pit were less than 10 µm in length. After a layer removal of 201 µm depth (at the pit base), a crack, ~50 µm in length, can be observed at the left side of the pit. Considering the difference in crack size from the base of the pit upwards it would be inferred that the crack initiated near the pit base.

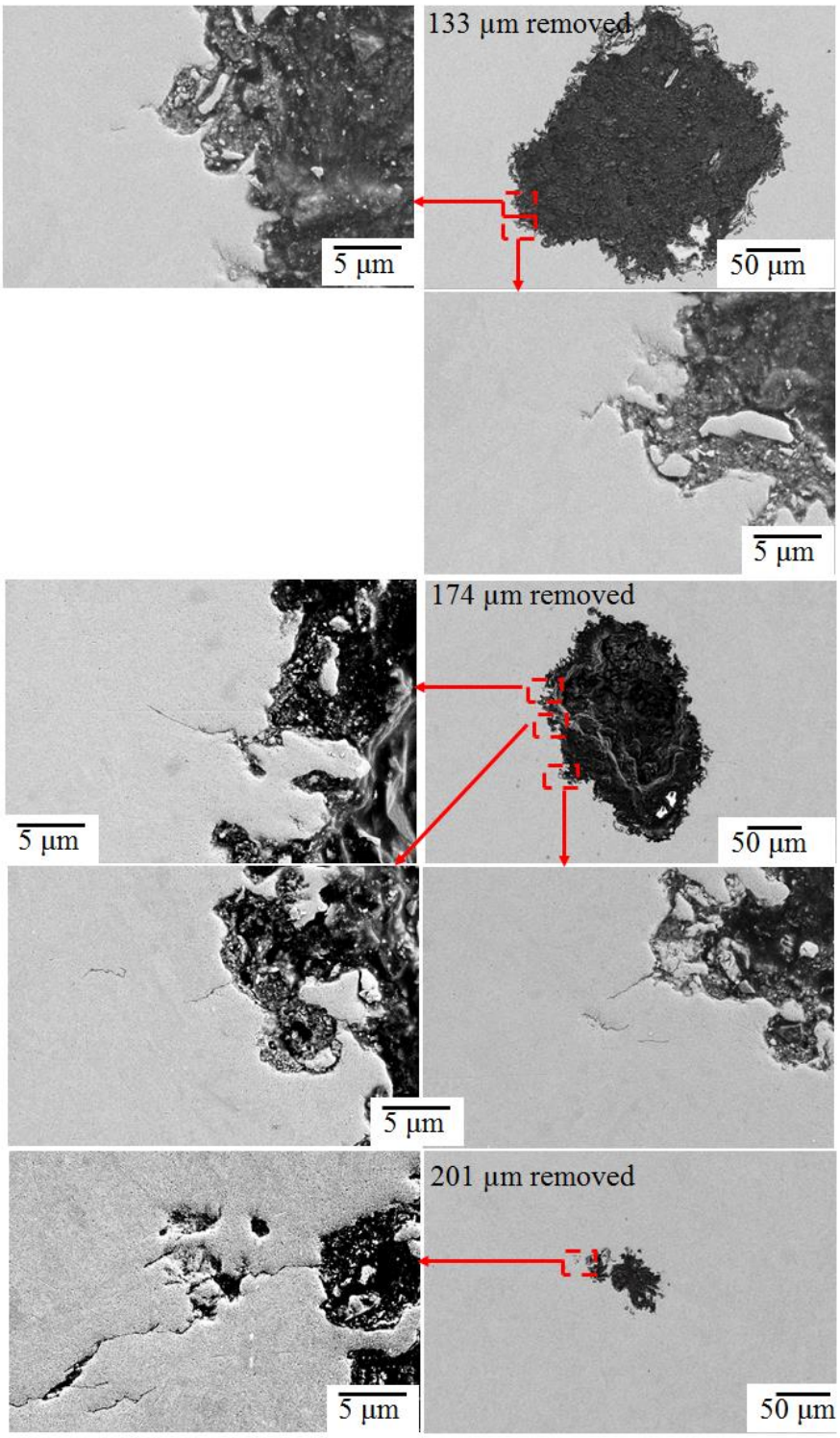

Figure 6: SEM images of a pit of 209 µm depth and the corresponding cracks after serial sectioning.

So, how do we explain these observations?

The measured longitudinal residual stress profile for the shot-peened specimen is shown in Figure 7. The compressive stress was about -700 MPa close to the surface and extended to a depth of about 350 µm or so; albeit below a depth of 225 µm the absolute magnitude was less than 100 MPa and close to the uncertainly level in X-ray diffraction measurement. This stress distribution should be compared with a maximum applied tensile stress in fatigue of 663 MPa.

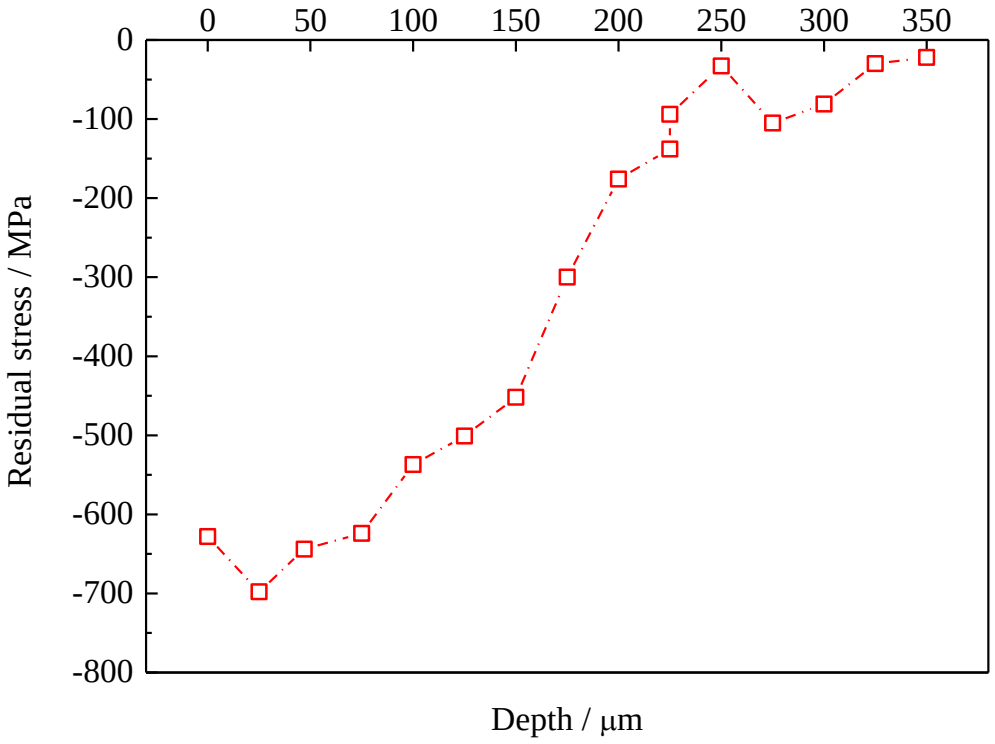

Figure 7: Longitudinal residual stress profile determined by X-ray diffraction.

To understand better the impact of the pit on the stress distribution, Finite Element (FE) analysis of the stress and strain distribution around a pit was undertaken as described in Reference 9 assuming a truncated spheroid for the pit shape with the pit mouth opening equal to the pit depth. The analysis was approximate in three ways: only longitudinal stress was accounted for; the variation in material properties induced by peening was ignored, which would influence the stress distribution (though for reasons articulated in [9] that would not be too significant a factor); the pit was ideally smooth, though the truncated spheroid geometry did match the macro-geometry of actual pits. Hence the results should be considered indicative only; the quantitative aspects would be less reliable.

Figure 8 to Figure 10 show the results of FE analysis (with 663 MPa applied tensile stress and residual compressive stress data as shown in Figure 7), carried out for pits of three depths: 50 µm (Figure 8), 150 µm (Figure 9) and 250 µm (Figure 10). Note that the colour coding generated by Abaqus is not consistent for the three figures. For the 150 µm and 250 µm deep pits, the maximum stress and strain are at the pit base with the maximum stress being over 900 MPa for the 250 µm deep pit (cf. yield stress of 819 MPa). The data show that the stress and strain concentration associated with the 50 µm pit is relatively small. There is an apparent high strain, relative to the base, local to the pit mouth, but this is likely computational uncertainty associated with meshing.

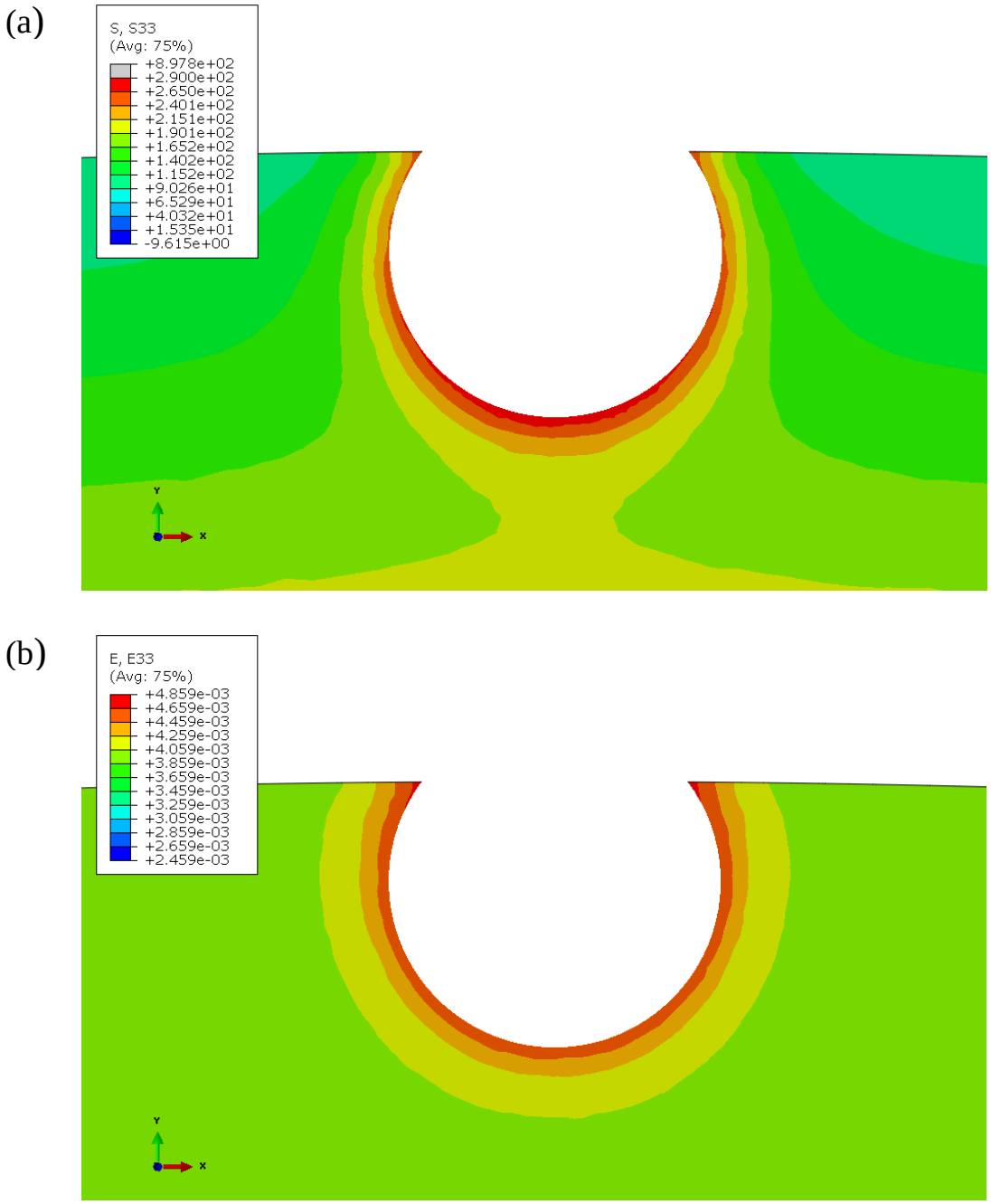

Figure 8: Cross-Section view of stress (a) and strain (b) around 50 μm deep pit calculated with longitudinal (z-direction) residual compressive stress (profile shown in Figure 7) and 663 MPa applied tensile stress.

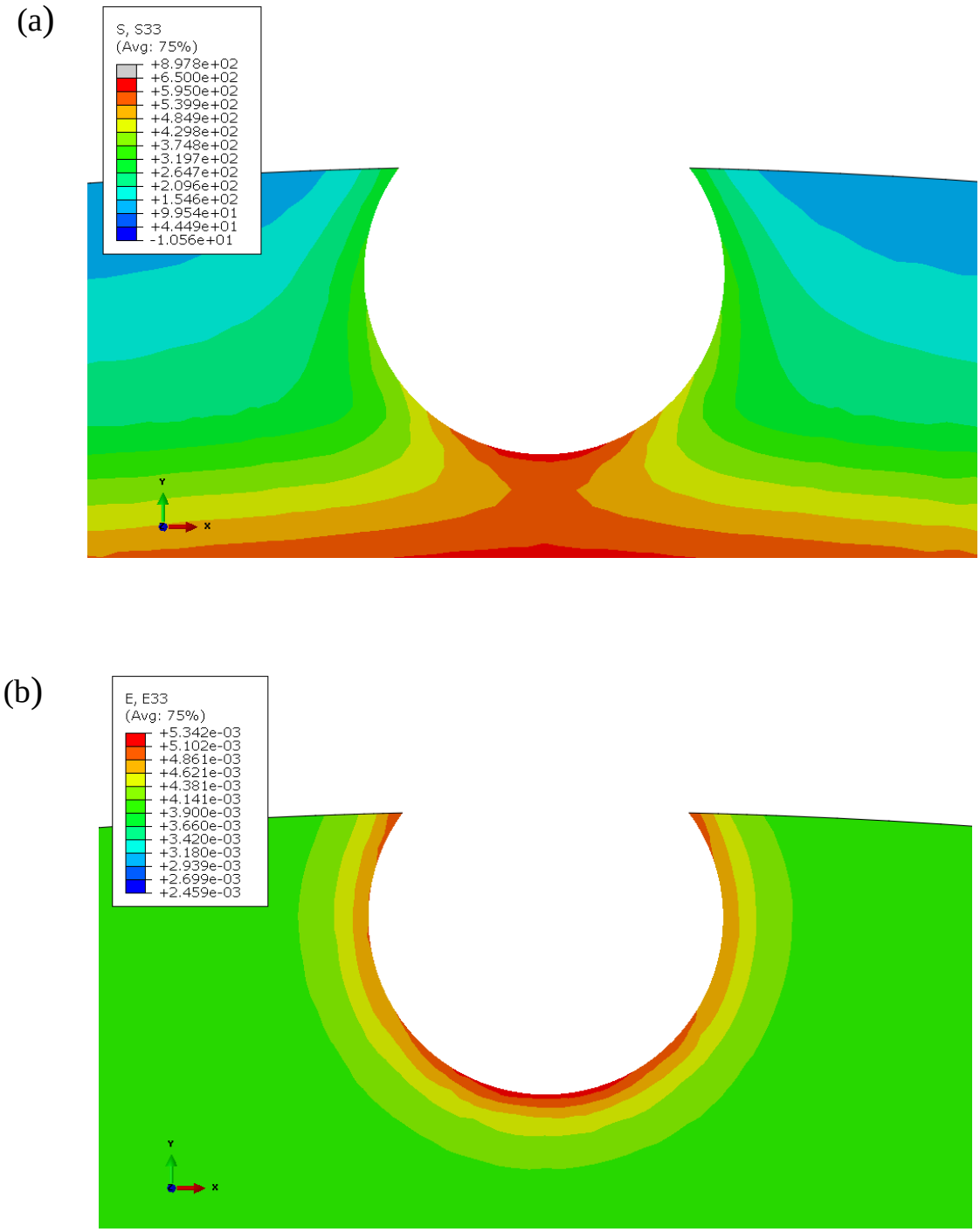

Figure 9: Cross-Section view of stress (a) and strain (b) around 150 µm deep pit calculated with longitudinal (z-direction) residual compressive stress (profile shown in Figure 7) and 663 MPa applied tensile stress.

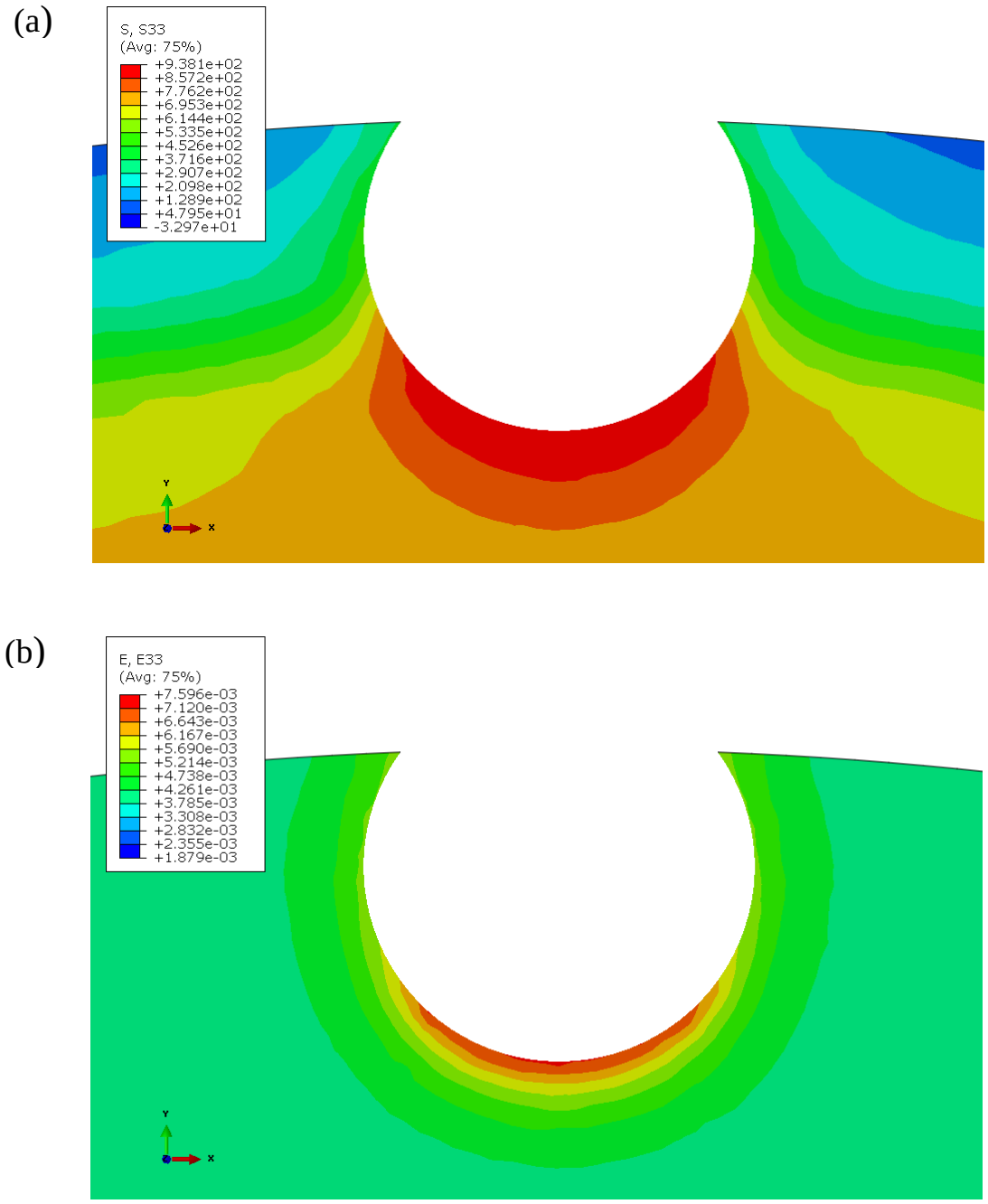

Figure 10: Cross-Section view of stress (a) and strain (b) around 250 μm deep pit calculated with longitudinal (z-direction) residual compressive stress (profile shown in Figure 7) and 663 MPa applied tensile stress.

Consequently, based on the FE modelling results, it would be predicted that cracks are more likely to initiate near the pit base certainly for the 150 and 250 μm deep pits where there is greater tensile stress and strain, in contrast with the results in Figure 4.

There was no evidence of significant stress relaxation during fatigue testing of the shot-peened steel so that is not a factor. However, for a real pit, the shape will be irregular with microtopographical features (as shown in Figure 1, Figure 5 and Figure 6), which would be expected to affect the stress/strain distribution [7] and consequently the crack initiation site. The counter argument is that these features prevail at different depths as is evident from Figures 5 and 6. The surface of the specimen is very rough

(Ra of 2.7 μm) and that could be significant in encouraging crack development near the surface. The surface is a heavily deformed region with a nanocrystalline top layer that in some locations has been measured to be about 15 μm. Fatigue crack initiation is usually more difficult the smaller the grain size. However, the heavily deformed region below the nanocrystalline layer and the new surface generated by the pit may encourage sub-surface crack development below the nanocrystalline layer.

The results in this study contrast somewhat with those reported previously [4-6]. Hornbach et al. [4] and Kubota et al. [5] used notches prepared by electric discharge machining to a depth of about 250 μm or greater as crack initiation sites but the shapes were not very similar to pits so direct comparison with the current study is not so meaningful. Nevertheless, they deduced from the fracture surface that cracks initiated at the base of the notch. Garcia et al. [6] endeavoured to identify crack initiation sites from artificial pits in unpeened and shot-peened Al 7075-T7351 and unpeened and shot-peened 4340 and D6AC steel by crack front marking. Crack front marking of aluminium alloys is usually more effective than for steel and in this case there was clear evidence for crack initiation near the pit base for the unpeened alloy. For the peened aluminium alloy the first crack front marker extended over a more significant region of the pit so that the origin of cracking was less well defined but it was evident that the crack did not extend to the surface at this stage. The location of the crack initiation site for shot-peened 4340 steel and shot-peened D6AC steel was less clear as the first crack front marker was too advanced to enable precision. Nevertheless, the authors concluded that the majority of cracks in both alloys initiated at the pit base. In comparing with the current work, it is notable that the pits investigated by Garcia et al. were roughly hemispherical in contrast to the truncated spheroid for the martensitic stainless steel in our work. Pit shapes in low alloy steels and stainless steels would be expected to be different. Also, the pit depths ranged from about 0.5 mm to 2 mm, much greater than the maximum pit depth of about 250 μm adopted in the current study, and the pits in the low alloy steels were much smoother as a consequence of the nitric acid induced dissolution.

4 CONCLUSIONS

A serial sectioning procedure has been applied on a shot-peened 12Cr martensitic stainless steel with pit depths varying from 30 μm to 240 μm to investigate the impact of pitting on the fatigue crack initiation site.

- Multiple cracks were observed on each pit after interrupted fatigue testing with the exception of the pit of 31 μm depth.
- Fully-developed cracks (surface-breaking cracks extending beyond the pit base) and non-fully-developed cracks were both observed. If the longest crack at each side of the pit was assumed to be the "dominant" crack, the non-fully-developed "dominant" cracks commonly did not initiate from the pit base, contrary to normal expectations, though one example was found.
- FE analysis has been carried out to characterise the stress/ strain distribution on specimens with pits of depths: 50 μm, 150 μm and 250 μm. In all cases, the greatest stress/strain was observed near the pit base.
- There was no evidence of residual stress relaxation.
- A clear explanation for the observations has not emerged but it is proposed that a combination of heavily deformed sub-surface of the shot-peened material with microtopographical features of the pit may make that region more susceptible to fatigue crack initiation.
- It is important not to generalise our own results but to emphasise that the location of crack initiation around the pit would be expected to be a sensitive function of the nature of the alloy, pit depth and shape (including microtopographical features), applied stress and the magnitude and depth of residual stress profile. What is clear is that the presumption that the crack will start from the pit base because of the residual stress gradient may not necessarily be correct for some systems.

5 ACKNOWLEDGEMENTS

This work was conducted as part of a joint venture between the United Kingdom Department for Business, Energy and Industrial Strategy (BEIS) and an industrial group comprising S. Fenton (Uniper Technologies Limited, UK), D. Gass (Siemens), W. Hahn (EDF Energy), H. Pitts (HSL), S. Osgerby (GE Power), P. Reed (U. Southampton) and A. Rowe (RWE npower).

6 REFERENCES

[1] V. Azar, B. Hashemi, M.R. Yazdi, The effect of shot peening on fatigue and corrosion behavior of 316L stainless steel in Ringer's solution, Surf. Coat. Technol., 204 (2010) 3546-51.
[2] M.N. James, M. Newby, D.G. Hattingh, A. Steuwer, Shot-peening of steam turbine blades: Residual stresses and their modification by fatigue cycling, Fatigue 2010, 2 (2010) 441-451.
[3] S.P. Wang, Y.J. Li, M. Yao, R.Z. Wang, Fatigue limits of shot-peened metals, Journal of Materials Processing Technology, 73 (1998) 57-63.
[4] D.J. Hornbach, J.E. Scheel, Improving corrosion fatigue performance & damage tolerance of 410 stianless steel via LPB, in proceedings of "ASME 2012 International Mechanical Engineering Congress and Exposition" Houston, Texas, USA, pp. 737-744.
[5] M. Kubota, T. Suzuki, D. Hirakami, K. Ushioda, Influence of hydrogen on fatigue property of suspension spring steel with artificial corrosion pit after multi-step shot peening, ISIJ Int., 55 (2015) 2667-76.
[6] D.B. Garcia, R. Forman, D. Shindo, Experimental evaluation of fatigue crack initiation from corroded hemispherical notches in aerospace structural materials, Fatigue Fract. Eng. Mater. Struct., 35 (2012) 122-40.
[7] L. Wright, A. Turnbull, FE analysis of stress and strain localisation associated with microtopographical features in corrosion pits, NPL Report MAT 78, 2015.
[8] A. Turnbull, S. Zhou, M. Lukaszewicz, Environmentally Assisted Small Crack Growth, Procedia. Materials Science, 3 (2014) 204-8.
[9] A. Turnbull, L. Crocker, Finite Element analysis of stress distribution around corrosion pit in shot-peened steel, NPL Report MAT 81, 2016.